Thermo Structural Analysis of Biomass Combustion Steam Generation Heat Exchangers Using Three Dimensional Numerical Modelling

Kannie Winston Kuttin [a,b*], Enock A. Duodu [c], Augustine Mensah [c] and Naziru Muhammed [c]

[a] *Institute of Clean Coal Technology, East China University of Science and Technology, Shanghai -200237, China.*
[b] *Engineering Research Center of Resource Utilization of Carbon-containing Waste with Carbon Neutrality, Ministry of Education, China.*
[c] *Department of Automotive and Mechanical Engineering, Akenten Appiah-Menka University of Skills Training and Entrepreneurial Development, Kumasi, Ghana.*

Authors' contributions

Original Research Article

ABSTRACT

Biomass with all its positive characteristics contains some elements and compounds that react negatively with stainless which are known for its usage in high temperature, corrosive prone and, hash environment. Therefore, it is pertinent to comparatively study the strength of various corrosive

_____

*Corresponding author: Email: zigoshone@gmail.com;

resistance metals to be able to have an alternative to stainless steel. The purpose of this study is to model and simulate a three-dimensional steam generating boiler plant heat exchanger for a biomass firing process. In the study, inlet temperature and operating temperature of shell and tube sides are taken as input parameters with a square pitch bundle arrangement. The heat transfer analysis is done by considering hot flue gas inside the tubes and steam on shell side to determine the thermal stress, strain and deformation distributions in the tubes and shell of the heat exchanger. The study also presented time-history analysis of the both shell and tubes to ascertain the material reactions within the specified time range. The comparison of deformations and the equivalent strain rate between the two designs indicated an excellent performance of the AL6XN over the 306L stainless steel. The strain amplitude for PMX110 and WKX110 sequentially dropped from 903 to 496 and 621 to 332 between the temperature range of $100 - 10000C$ respectively. The maximal equivalent strain values for the shells and tubes were 2.238e-003 and 1.294e-004 for PMX110 and 1.490e-003 and 3.212e-004 for WKX110 respectively. The highest deformation in both PMX110 and WKX110 were estimated as 6.729e-004 and 6.131e-004 for the shells and 1.441e-004 and 1.328e-004 for tubes respectively.

1. INTRODUCTION

One of the essential resources for the economic growth of every nation is thermal energy Pandiyarajan et al., [1]. Saidur et al. [2] report that a nation's energy consumption increases as its economy and population expand. Increasing fuel prices are compelling industries and governments to increase their energy efficiency [2,3]. The situation is worsening because of increasing petrol prices and environmental problems caused by greenhouse emissions [4]. Biomass, as a versatile and renewable energy source derived from organic materials, plays a crucial role in advancing the United Nations Sustainable Development Goals (SDGs). By promoting clean and affordable energy (SDG 7), biomass supports rural electrification and reduces dependence on fossil fuels, contributing to climate action (SDG 13). Its implementation fosters economic growth (SDG 8) through job creation in agriculture and energy sectors while enhancing food security (SDG 2) by utilizing agricultural residues. Biomass energy also promotes good health and well-being (SDG 3) by reducing indoor air pollution from traditional cooking methods and supports gender equality (SDG 5) by alleviating the burden of fuel collection on women and girls. Additionally, it encourages sustainable land use and biodiversity conservation (SDG 15), making biomass a pivotal element in achieving a sustainable and equitable future. A boiler is a confined vessel used for changing fluid to steam, typically water. Heated or vaporized fluid is used in various heating operations and applications, including cooking, sanitizing, heating water, heating the entire structure, and generating electricity using turbines. Boilers are being used for new purposes as a result of rigorous regulations on pollution, the use of alternative fuels and improvements in other disciplines such as water chemistry and materials. Secondly, as market competition increases, boiler designs become increasingly extreme, necessitating a deeper comprehension of dynamical behaviors. Energy efficiency, Safety and the boilers' dynamic performance are given more consideration due to the stringent global manufacturing regulations.

The most common type of heat exchangers are the Shell and tube type, which found it application in refinery of oil and processing of chemicals due to their suitability for high pressure applications [5]. Shell and tube heat exchangers are employed in numerous industries, including refrigeration, treatment of wastewater, production of beer and wine, nuclear power, petroleum refining, and steam generation facilities, due to their low cost and simplicity of maintenance [6]. A heat exchanger in a furnace is a component that facilitates the heat transfer between two fluids or substances without combining them Guerras et al., [7]. (Westerlund et al., [8]. The working fluid of a boiler receives it energy from energy created by the boiler from its gas supply. There are varieties of heat exchangers, such as brazed plate and shell and tube types, differing in terms of size, efficacy, footprint, and cost. The type of heat exchanger is determined by the output of the boiler.

Large-fired exchangers are frequently utilized in industry to produce steam, and since they typically account for a considerable portion of the total fuel consumed by a facility, they have

garnered a great deal of interest from business and academic communities. In addition, the readiness of steam at appropriate conditions and flow rates is a crucial element in the operation of any steam generating facility. Depending on the fluid type, viscosity, its phase, pressures, temperature, chemical composition, and other thermodynamic variables, the type and size of heat exchanger used in a process can be modified to suit the needs of the system.

Heat exchangers are also used as economizers to recover heat lost in industrial processes or that is being exhausted from one heat stream in order to heat another heat stream. By utilizing heat exchangers to provide heat to other streams as opposed to a costly and external source which is environmentally hazardous, businesses can save a substantial amount of money. Extensive research has been conducted on heat exchangers, including computational and experimental techniques that account for both the fluid and metallic components.

Applying biomass and waste in generating steam is a preferable option to consuming traditional fuels given that the combustion of biomass does not result in any net CO_2 emissions. The tendency of these fuels, particularly in waste-fired facilities, to cause corrosion of superheaters at high temperature is a significant issue. However, to prevent the deterioration power plants fired by these fuels operate at a significantly lower steam temperature. As a consequence, the production of steam becomes substantially less efficient. Improving the corrosion resistance of metals is essential for increasing the efficiency of steam in these plants.

The superheaters constructed with corrosion resilient alloys frequently depends on the synthesis of chromium-rich corundum oxide to prevent corrosion. This protective oxide, which is frequently a mixture of chromium oxide and iron, derives its protective qualities from the chromic oxide quantity in the composition; mixtures with higher Chromium to iron ratio have more protective qualities. As a consequence, operations that involve the reduction of chromium oxide are typically hazardous, yielding iron-rich chromium deficient with inadequate protective properties. As proved by Asteman et al. [9]. one of these mechanisms involves the interaction of water and oxygen compounds to generate acidic chromic gas. When the 304L alloy is exposed to these combinations, local corrosion with a double oxide composed of an external developing

hematite film and an inner growing spinel oxide occurs [10]. Alkaline, chlorine, calcium, and SO_2 concentrations are elevated in high-temperature environment of combustion of waste and biomass [11].

As a result, alkali chloride ions deposits are prevalent in superheater tubes. The corrosion deterioration of alkali chlorides at high temperatures towards stainless steels has been extensively studied [12]. Numerous efforts have been made Brostrom et al., [13] to decrease corrosion in furnaces by modifying the fireside environment chemistry to prevent the deposits of alkali chloride formation. These endeavors have achieved some measure of accomplishment. According to Viklund et al. [14], sulfur-containing compounds added to the fuel decreased the rate of corrosion by 50–70% under these conditions. However, current research on stainless steel corrosion promoted by potassium-chloride in high temperature systems by Pettersson et al. [15] indicates that potassium ions play the most significant role in the early stages of corrosion. According to a study of deposit compositions in coal-biomass combustion systems by Simms et al., [16], high chlorine and potassium content in biomass fuels, can result in high potassium-chloride deposits, particularly in combustion systems of low temperature (such as fluidized bed systems) fired exclusively on biomass. To determine the maximum available work output of a STHE, Alamu et al. [17] conducted exergy and energy analysis by varying operating parameters and configuration of the space heaters connected to the STHE for space heating lab-scale fluidized-bed combustion reactor. It was observed that exergy loss increased with increasing flue gas flow rate from 46.8–57.6 kg/h and with increasing ambient temperature from 8.8 °C to 25 °C. Mori et al. [18] conducted corrosion behaviour analysis on T91 and TP347HFG alloys in a simulated agricultural product combustion environment at 600°C (up to 1000h; 100h cycles) to understand the effect of parametric variations on fireside corrosion to be able to alter the degradation of heat-exchangers. It was reported that, the deposit with lowest KCl showed lowest corrosion damage, while the highest KCl deposit showed more aggressive behaviour. To determine the mechanical strength of these materials, the present study numerically compares 304L stainless steels to AL6XN, which is known to perform well in such environments and whose heat transfer capability has been numerically tested and found to be greater than that of 316 stainless steels.

2. MATERIALS AND METHODS

2.1 Materials

AL-6XN was used for the proposed heat exchanger shell, tube buddle, baffles and tube sheet, while 304L stainless steel was used for the Log and Lumber Limited (L.L.L.) PMX110 Prime boiler superheater heat exchanger and its entire elements (baffles and tube sheet). The heat exchanger model was created based on dimensional parameters in Table 1, using the commercial CAD application Solidworks Product 2019. For numerical simulations, ANSYS Workbench (mechanical) version 2020R1 commercial software was utilized.

2.2 Methods

According to Nsofor et al. [19], temperature and pressure are the two most influential variables in the design of heat exchanger systems. Several other parameters, such as initiation, cessation, upset, dry-out, external tension from supports, pulsing pressure, wind loading, seismic load, etc., also have extensive effect on the heat exchanger's performance. The following considerations were made when designing a heat exchanger: (i) Pressure and temperature of operation, (ii) Conceive of pressure and temperature, (iii) The required heat transfer rate or heat discharge in its entirety, (iv) Flue gas inlet/outlet temperatures, and (v) Fluid outlet and inlet temperature.

The heat exchanger mechanical datasheet was created by using this information in accordance with the Tubular Exchanger Manufacturers Association (TEMA) standards. The heat exchanger design process is an open-ended design issue, making use of less constraint than available variable parameters. Some of these factors may be modified in order to design a heat exchanger that is both economical and efficient.

Some process variables, such as the rate of flow of process fluid, the inlet temperature, design and operating pressure values, the highest allowable pressure decline, etc., were fixed. Calculations and simulations utilized these variables as constant inputs. Utilizing the performance data of an operational heat exchanger of the same type and processing the same solution, the total coefficient of heat transfer was calculated.

2.3 Numerical Design Procedure

Using the Bell-Delaware and Kern methodologies, thermal and hydraulic analyses were conducted independently for the tube stream and the shell stream [20]. The Bell-Delaware approach is the utmost used method for calculating the thermal and hydraulic quantities of the shell side [21], whereas the Kern method is the most straightforward method for calculating the physical dimensions of the various elements [22].

2.3.1 Number of tubes

The tubes internal rate of flow (m_t) is affected by the fluid's density (ρ_t), its velocity (u_t), the cross-sectional flow area (A_c), and the number of tubes (N_t) and is determined by (1).

$$m_t = \rho_t u_t A_c N_t \tag{1}$$

The number of tubes is estimated by (2) by substituting A_c by $\pi d_t^2/4$ for Ac in Equation (1), where tubes internal diameter is denoted by d_i.

$$N_t = \frac{4m_t}{\rho_t u_t \pi d_t^2} \tag{2}$$

2.3.2 Tube-sheet mean metal temperature

Un-tubed and tubed portion of tube-sheet is determined by (3) and (4)

$$T_{TS} = \frac{T_T - T_S}{2} \tag{3}$$

$$T_{TS} = T_T + (T_S - T_T)\frac{(\eta - F)}{(A/a)\left(1 + \eta \dfrac{h_T}{h_S}\right)} \tag{4}$$

Where,

T_T= Tube stream fluid temperature, K

T_S=Shell stream fluid temperature, K

h_T=Tube stream coefficient of heat transfer

h_S =Shell stream coefficient of heat transfer

$$\eta = \frac{A}{aK}\left[\frac{1 + \dfrac{A}{aK}\tanh(K)}{\dfrac{A}{aK} + \tanh(K)}\right]$$

$$K = \sqrt{\frac{AhTL}{a12k}} \deg rees$$

where k = tube-sheet metal thermal conductivity = W/(m⁰K)

L= tube-sheet thickness, meters

$$F = \frac{1}{\cosh(K) + \dfrac{aK}{A}\sinh(K)}$$

(5)

for square pitch

$A = \pi dL$

$a = p^2 - \pi d^2/4$

d = tube ID, meters

P = tube pitch, meters

According to Jorge et al. [23], the equivalent diameter is determined by dividing the wetted perimeter by four times the minor total flow area as spread out on the tubesheet for all pitch configuration.

Table 1. Model parameters of the heat exchanger

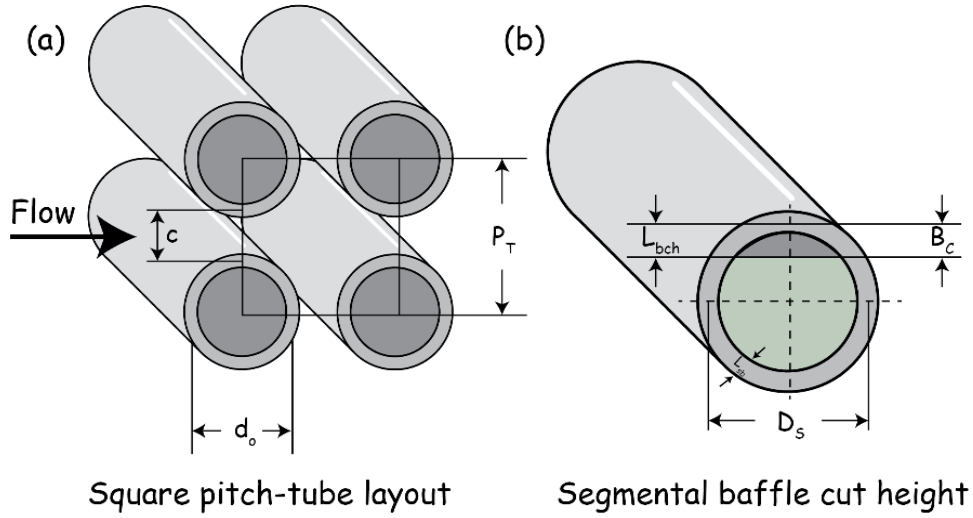| Parameter	Value
Tube exterior diameter	120.7 mm
Tube interior diameter	110.7 mm
Tube to tube center distance	160.5 mm
Pitch	Rectangular
Length of tubes	4209.73 mm
Number of baffles	2 and 5 Nos.
Tubes passes	1

Fig. 1. a. Square pitch-tube layout b. Segmental baffle cut height

As shown in Fig. 1a, the square pitch is determined by (6)

$$D_e = \frac{4\left(P_T^2 - \dfrac{\pi d_0^2}{4}\right)}{\pi d_0}$$

(6)

Where d_o is the tube's outer diameter.

The number of channels at the shell's centerline was determined by (7).

$$N_t = \frac{D_S}{P_T}$$

(7)

Where

N_t = tubes number

D_s = shell internal diameter

P_T = tube pitch

$$A_S = \frac{D_s}{P_T} CB$$

As = area of cross-flow of tube bundle

Ds = shell internal diameter

C = clearance of adjacent tubes

B = baffle spacing

Tube clearance (C) is the expression as

$$C = P_T - 2_{ro} = P_{To} - d_0$$

2.3.3 Number of baffles, N_b

To calculate the total number of cross passages and window turnarounds, it is essential to determine number of baffles, N_b. When necessary, N_b is calculated using the sum of spacings of all the baffles L_{ti} and the spacing of the baffle B [24]. The requisite exchanger length and permitted baffle count were determined using (8)

$$N_b = \frac{L_{ti}}{B} - 1 \tag{8}$$

2.3.4 Baffle segmentation represented as a percentage of D_s B_c (%)

Assuming the baffle segment is centered inside the shell's inner diameter Ds, the relationship between the segmental baffle cut height L_{bch} (mm) and B_c is shown in Fig. 1b as (9) in percentage.

$$B_c = \left(\frac{L_{bch}}{D_s} \right) (100) \tag{9}$$

The clearance L_{sb}, or minor variance between the baffle and shell diameters, is essential. A TEMA chart depicting the suggested standard values of B_c against the ratio of spacing of the central baffle B and the inner shell diameter Ds is available for design purposes and/or for confirming the provided values [24].

2.3.5 Heat exchanger length

Using equation (10), the heat exchanger length is calculated.

$$L = \frac{A_f}{N_t \pi d_o} \tag{10}$$

Where

L = heat exchanger length

d_o = tube external diameter

N_t is the total number of tubes

2.3.6 The overall coefficient of heat transfer

The overall coefficient of heat transfer for clean surface (U_c) is given by (11)

$$\frac{1}{U_c} = \frac{1}{h_o} + \frac{1}{h_i} \frac{1}{d_i} + \frac{r_o \ln(r_o / r_i)}{k} \tag{11}$$

k = thermal conductivity of the tube material

h_o = coefficient of heat transfer of the shell-stream

h_i = coefficient of heat transfer of the tube-stream

r_o = external radius of the tube

r_i = internal radius of the tube.

The coefficient of heat transfer for a stained surface U_f was calculated using the (12), taking the total fouling resistance R_{ft} into account:

$$\frac{1}{U_f} = \frac{1}{U_c} + R_{ft} \tag{12}$$

2.4 Meshing of Models

Using the finite element mesh, the model is subdivided into smaller regions so that a set of equations could be solved there. Despite the small size of the exchanger, the majority of its geometry was discretized using polyhedral mesh elements, which is sufficient to provide a satisfactory high resolution. In addition, only half of the shell was mesh because it is symmetric along the y-axis. Due to the importance of heat

transmission in this region, the tubes are mesh with a particular degree of finesse. To ensure a seamless rate of volume change and compute each local height and total height, the smooth transition option is used to localize the size of the tetrahedral element sections. The minimum capacity limit and skew tolerance are set at 1 each. When Curvature and Proximity Refinement is set to Yes, the mesh is automatically adjusted based on geometry curvature and proximity. This resulted in smaller components on areas of high curvature or between minute gaps, and larger components on flat, planar surfaces. The models are meshed using quadratic/triangular elements with six nodal phases, a generalized planar strain approximation, and decreased integration. A quadratic polynomial form offers high order interpolation to the dislocation field and, subsequently, a more precise distribution of strain and stress. The meshing has a substantial impact on the final outcomes, particularly when analyzing tension distribution at tube-baffling contacts. The models were discretized with extremely small element sizes of 0.3 to improve the accuracy of the final result.

2.5 Loading Conditions and Boundaries

The working fluid temperatures on the both shell and tube streams were 30°C and 1000°C, respectively. Temperature fields were estimated using a starting temperature of 300°C, and the results are then used to compute the stress in the structural model. The stress was calculated by utilizing the thermal expansion base on temperature-dependent coefficient. Consequently, model's heating expansion is the only factor that contributed to the final stresses from the location temperature to the operational temperature. As part of the thermal loading of both streams, the entire system is subjected to a uniform temperature after the thermal cycle. In a single cycle, the burden is comprised of three phases. The procedure entails heating from 30°C to 1000°C in the first 300 seconds, maintaining that temperature for 7200 seconds, and then reducing from 1000°C to 30°C. The working pressures on the tube and shell streams are 3 MPa and 5 MPa respectively. In the computational analysis of stresses, the effect of welding is disregarded.

3. RESULTS AND DISCUSSION

3.1 Grid Optimization Analysis

Taking into consideration the result accuracy and fast solution convergence, four different computational meshing cells of 116216, 128672, 142174, and 152240 cells were considered for each of the two components meshing analysis on the stress and strain simulated results for tubes and shells. The percentage of variable change between 142174 and 152240 cells for tubes and shells was insignificant. Therefore, 142174 cells have been selected as the optimum grid cells for all performed simulations.
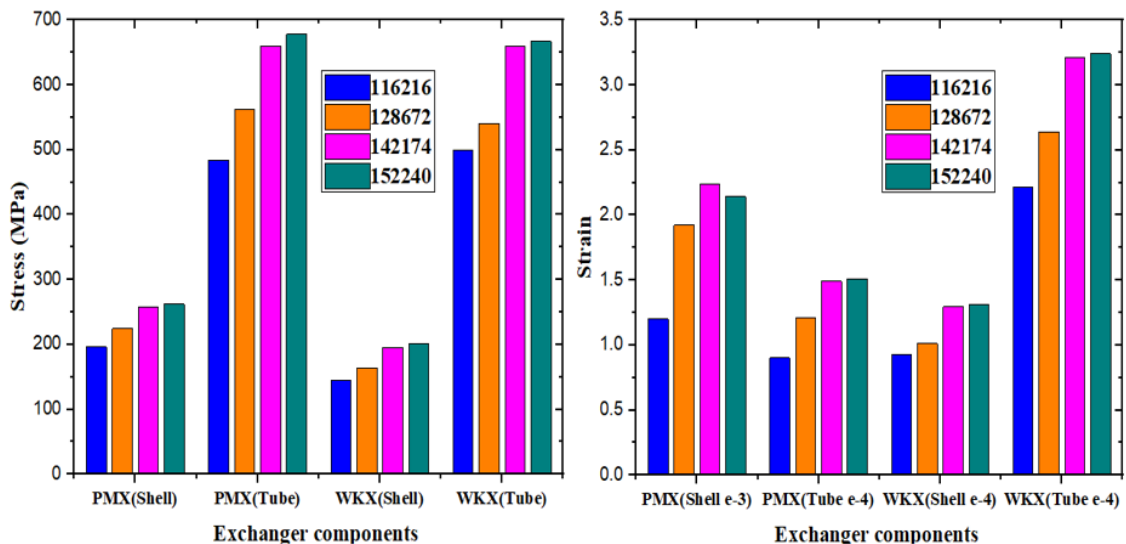

Fig. 2. Gas composition at the gasifier outlet for different mesh sizes

3.2 Thermo-structural Analysis of the Heat Exchangers

This simulation was conducted to compare the mechanical strength of the new design's AL-6XN material to that of the existing design's 304L stainless steel. Although the majority of the properties of the two materials are comparable the same, the addition of aluminum and increase in molybdenum whiles reducing the chromium content have altered the values of several crucial parameters, including increase in the young modulus of elasticity of AL6XN. The toxicity ratio might also because of the possible increase in molybdenum oxide at high temperatures due to the increase in molybdenum content.

The temperature, heat flux, and coefficient of heat transfer distributions are crucial for the heat exchanger, as these variables may compromise the tube's structural integrity. The interior and exterior surfaces of the tube reached maximum temperatures of 900 degrees Celsius. The tubes highest surface temperature may exceed the heat exchanger material selection's temperature presumption value (950 degrees Celsius). Near the discharge gas entrance, the innermost portion of the tube had a maximal heat transfer coefficient of 100 W/m²K. The external tube region with the highest coefficient of heat transfer was measured to be 70 W/m²K near to the flue gas outlet. Using the coefficient of heat transfer and temperature distributions on the heat exchanger tubes, the thermal strain and stress analysis was conducted.

3.2.1 Stress distribution

To demonstrate the heat exchanger tubes integrity, a thermal stress study was conducted taking into consideration the high-temperature sections of the tubes bundle close to the flue input and steam outlet regions. Taking the symmetry nature of the heat exchanger shell construction into consideration, half of the heat exchanger shell was analyzed. Figs. 3 and 4 depict the results of the Von Mises stresses on the PMX110 and WKX110 tubes and shells respectively. In both instances, the length of the tubes without baffles were subjected to the greatest tension during tube loading. On the other hand, the highest stress value of the WKX110 shell was identified at the flue gas' exit, whereas the highest stress value of the PMX110 shell was identified at the flue gas' entrance. Under temperature and pressure loading, the shells exhibited von-Mises stress values of 258

MPa and 195 MPa, respectively. These data indicated that these stress levels were lower than those allowed for thermo-pressure vessels. The tension distributions in both tubes and shells are comparable to pressure and temperature loading combination scenarios. The maximal von-Mises stress value for PMX110 and WKX110 tubes were determined to be 660 MPa and 659 MPa, which were below stress value allowable in this investigation, which is 697 MPa. The tubes of the heat exchanger were subjected to a stress evaluation on ASME Section VII scheme. The total membrane stress was 162 MPa, or 1.5 times the permissible stress value, which is less than the constraint limit. As a consequence, the tension condition of the heat exchanger met ASME requirements.

The exchanger thermal stress analyses were evaluated based on the allowable stress. According to ASME Section II, the greatest allowable stress value at 600 degrees Celsius is 667 MPa. The two cases were each subjected to three distinct stress analysis: pressure loading, thermal loading, pressure and thermal loading. Fig. 3 depicts the stress distribution of PMX110 and WKX110 tubes, with all stress components following a similar pattern over the upper surface. All tensions increased towards the periphery of the tube sheets before decreasing to their minimum value. Along the heat impact zone, the radial stress ratio for PMX110 and WK110 is 0.12 and 0.09, respectively. For the baffles, the radial stress surges progressively from the internal surface to the weld root of the tubes, where it reaches its maximum, before declining gradually away from the weld root. The hoop and axial stresses also decrease from the internal tube surface to the outer tube surface, reach their minimum value at the outer tube surface, increase to the weld root, reach their maximum value at the root, and then decline away from the heat-affected zone.

In this instance, consideration is given to the deformation resulting from the accumulation of stress and the relationships between restricted interfaces and the deformation distribution resulting from the continuous expansion of free edges. These analyses are also executed for various high amplitudes and demonstrate that the elemental composition of the materials has a substantial effect on the S_{22} stress distribution in the restricted interface regions of PMX110 and WKX110 tubes after subjected to high pressure and temperature. Restricted locations had the greatest influence on the stress state, and the

stress distribution induced by the fluctuating expansions also caused the two materials to have mismatched shapes. When these two forms of stress are combined, the tubes experience the maximum levels of tensile stress at their apex, where there are no baffles in the center and compressive load is concentrated. When the amplitude enhances and increases the behaviors of PMX110 and WKX110 tubes, a modest tensile stress was observed initially in the case of the low amplitude displacement at the incremental interval of 10, but this stress transforms progressively into a compressive stress. Except for when the amplitude is small (<10), the section of greatest compressive stresses was at the tubes' edges, and a considerable compressive zone is observed at the top for all amplitudes.

3.2.2 Thermal deformation analysis

In order to produce heat exchanger deformation contours for the tube and shell thermo-structural analysis, heat transfer coefficient and heat flux from the thermal analysis were imported as input to the thermal-structural deformation analysis. If the deformation of the tube bubble is not taken into account, thermal collapse caused by excessive pressure tension may occur at a higher operating temperature. To determine the total deformation of the shell and tube of both designs, the analysis was conducted in two steps: (1) a steady state thermal (heat transfer) solution was obtained to generate the nodal temperatures, and (2) a static structural solution was obtained by applying the nodal temperatures and the pressure loads. The contours of the resulting out-of-plane deformations of the entire surfaces of heat exchanger shells and tubes are depicted in Figs. 5 and 6. The deformation in both PMX110 and WKX110 were estimated as 6.729e-004 and 6.131e-004 for the shells and 1.441e-004 and 1.328e-004 for tubes respectively. As shown in Fig. 6, the tube sheets of both designs exhibited significant degree of distortion.
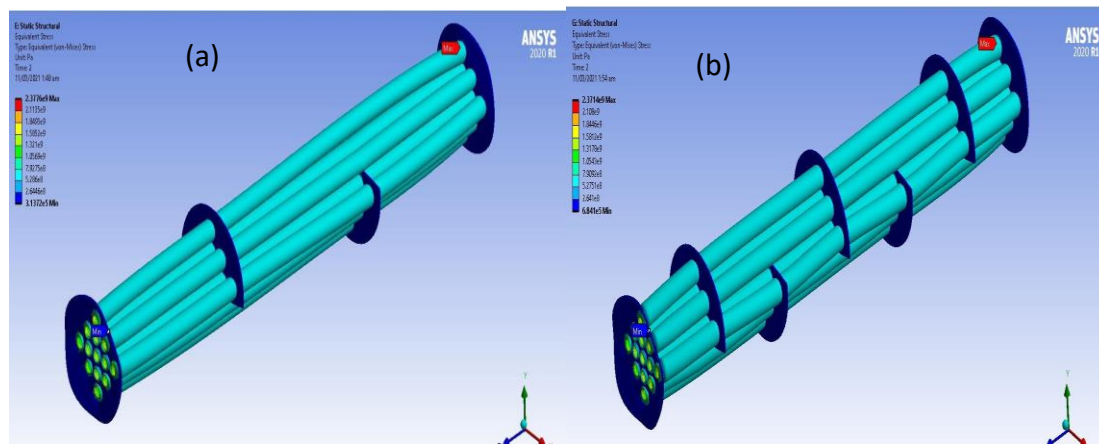

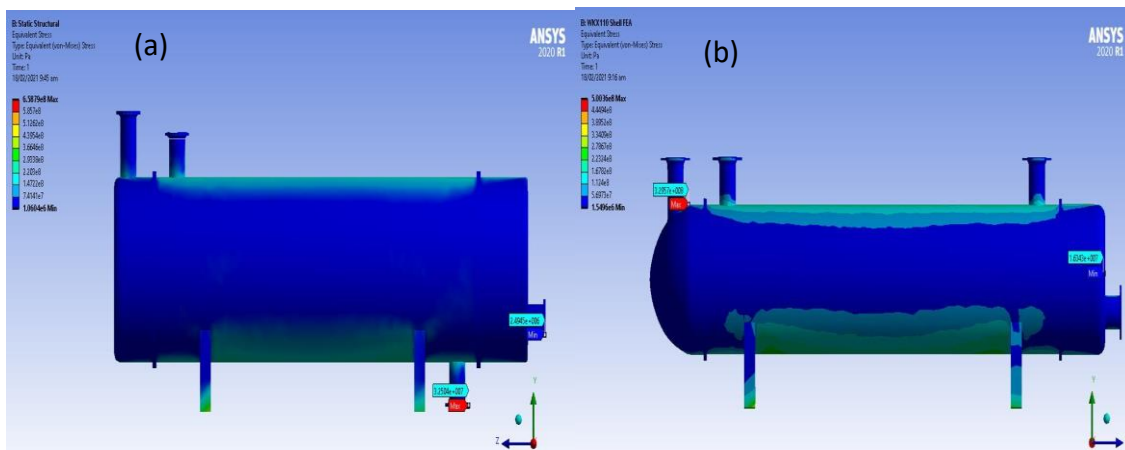**Fig. 3. Equivalent stress (von Mises) contour distribution of (a) PMX110 and (b) WKX110 Tube Bundle**

Fig. 4. Equivalent stress (von Mises) contour distribution of (a) PMX110 and (b) WKX110 Shell
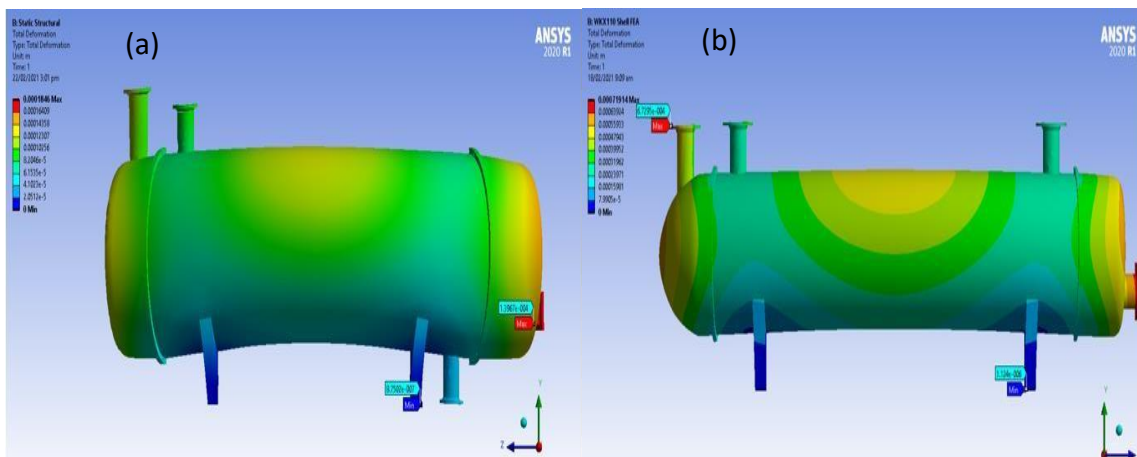
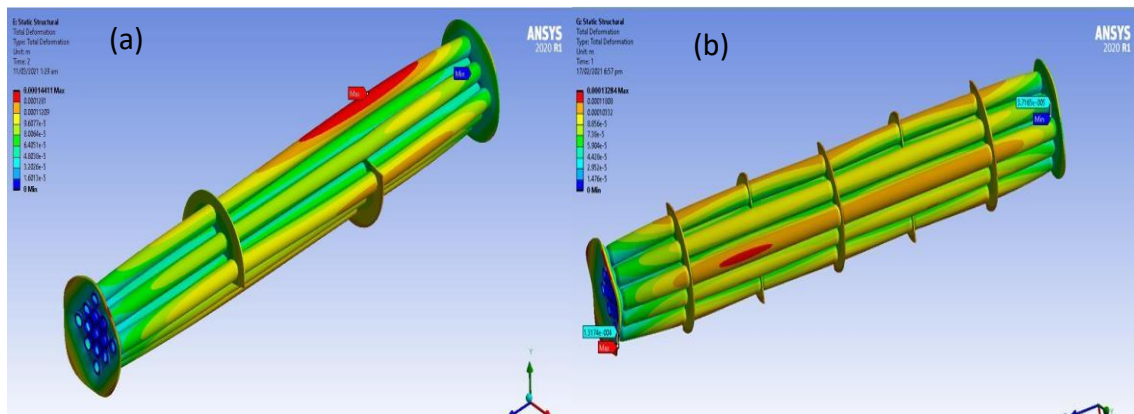**Fig. 5. Deformation contours of (a) PMX110 and (b) WKX110shell**

Fig. 6. Deformation contours of (a) PMX110 and (b) WKX110 tube bundle

The mass-volume ratio distortions were attributable to the perforations made in the tube sheet to accommodate the tube ends, the loading pressures at both ends of the tube bundle and the heating rate. As a fundamental tenet of mechanical design, the number of perforations will have an effect on the mechanical strength of any sheet material.

3.2.3 Effects of thermo-cyclic loading on strain

Figs. 7 and 8 depict the equivalent strains (von Mises) distributions of the tube and shell for PMX110 and WK110, respectively. There was a significant tube expansion in the high-temperature region near to the flue gas inlet, which progressively decreased. Strain distributions in both designs exhibited comparable distributions. At the flue gas intake point, the maximal equivalent strain values for the PMX110 shell and tube were 2.238e-003 and 1.490e-003, respectively, while the corresponding values for the WKX110 shell and tube were 1.294e-004 and 3.212e-004 respectively.

Under the same operating conditions, the effect of thermal loading on tube strain in the PMX110 and WKX110 demonstrates that repeated thermal cycles resulted in significantly greater tube strain than shell strain over the same time period. This phenomenon has a straightforward explanation: the distortion process commences above 800 °C and takes place during the heating dwell time t_1 at 900 °C as well as the step interval T_1 required to elevate the temperature from 800 to 900 °C. Strain occurs when the temperature decreases from 900° to 800°C, or at interval time t_2, when the cooling step commences.

Fig. 9 depicts the analysis of strain amplitude. The modulus-time is modified to attain the same stress-strain value limit for thermal loading. Since the distribution of the strains in this instance is virtually identical, differences in the minimum and

maximum strain values are insignificant. Our findings are consistent with Bialas [25] study on the influence of propagation of cyclic loading, which demonstrates that these discrepancies on minimum or maximum stress values were less than 2.5%. Intense thermal cycle loads generate a new set of stresses as a consequence of events such as growing defects by notch [26].
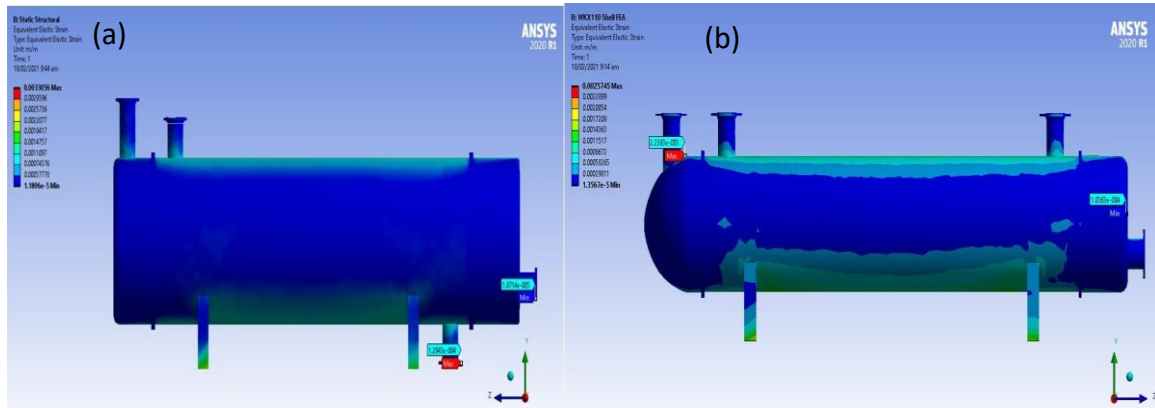

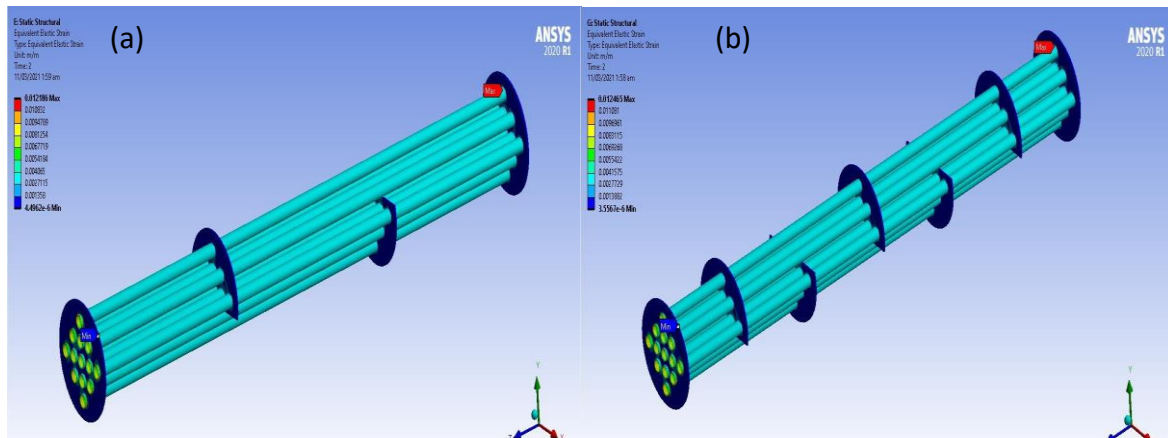**Fig. 7. Equivalent (von Mises) strain contours of (a) PMX110 and (b) WKX110 shell**

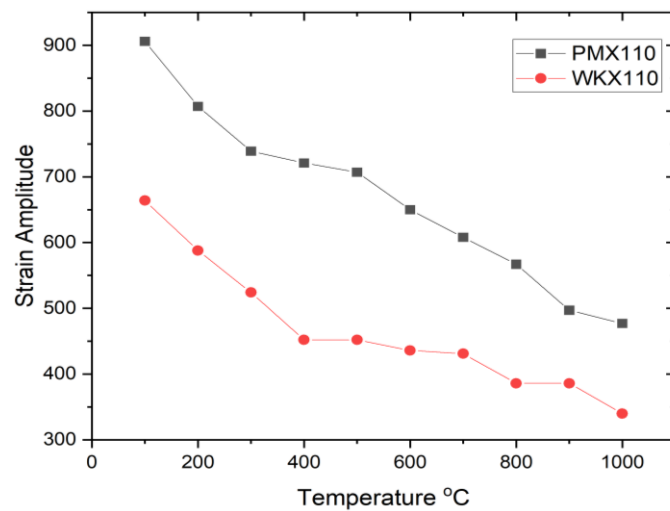**Fig. 8. Equivalent (von Mises) strain contours of (a) PMX110 and (b) WKX110 tube bundle**

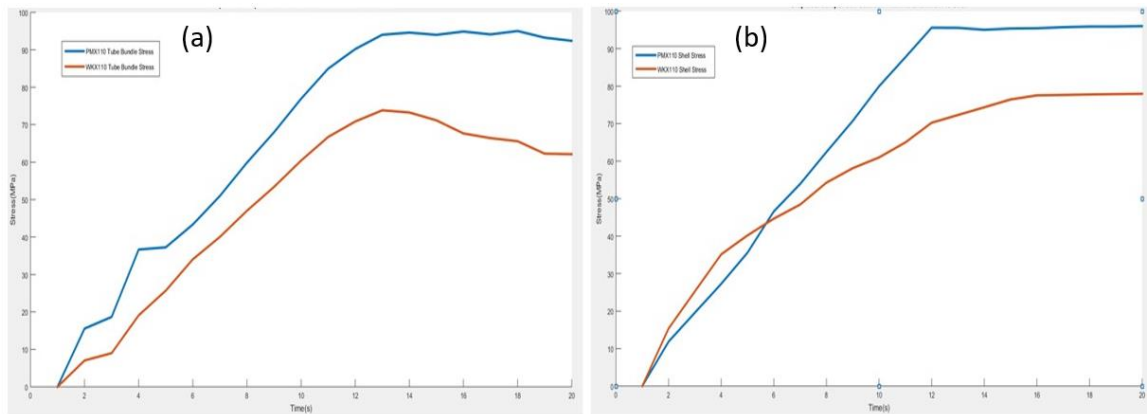**Fig. 9. Strain amplitude test analysis**

Fig. 10 a. Comparison of tube stresses b. Comparison of shell stresses

4. TIME-HISTORY ANALYSIS

In the time history technique used to model structural systems, there are a few predefined nonlinear components and linearly elastic elements. All nonlinearity is assumed to be confined to interactions between the heat flow and various nodes and components. Fig. 10 depicts what transpired between the two structures during the temperature rise in relation to time. The ability of WKX110 to maintain reasonable stress stability levels as the temperature rises over time bolsters the advantage of the temperature-reactional effect of the high nickel and low chromium content. The maximal stress-time curve point for both materials occurs at the same time interval (13 s), indicating the maximum temperature resistance of the materials.

As depicted in Fig. 10b, the curve of stress values versus time for the WKX110 shell is lengthy, whereas the PMX100 shell maintains an ascending gradient until attaining the maximal stress value. Earlier in the process, the two trajectories intersect, indicating a high temperature effect on both substances. For instance, as the thermal parameters increase, the PMX110 shell experiences high stress values, while the WKX110 shell maintains low stress stability value [27].

5. CONCLUSION

In this investigation, an optimal design of a heat exchanger (STHE) was proposed. This model of non-linear programming (NLP) rigorously adheres to the TEMA Standards. Thus, TEMA standards are adhered to for geometric features such as baffles number, diameter of tubes, diameter of shell, inner and outer tube diameters, length of tube, arrangement of tube, pitch of tubes, spacing of baffles, and passes of tubes to preventing the need to modify heat exchanger design parameters after the task has been completed.

A tubular heat exchanger was chosen due to its high resistance to harsh environments and negligible losses of pressure on both cold and hot streams. The utmost corrosion resistance, allowable stress, and availability were considered when selecting the heat exchanger material. Assessment was done to determine the total size of the heat exchanger using the tube-to-tube sheet criterion, and the results were compared to performance data for internal heat exchangers. It was decided to use a counter-cross flow configuration with dispersed tube array. The thermo-fluid flow study results were then applied to a thermal stress analysis. The heat exchanger condition was assessed according to the ASME protocol. The membrane's stress, strain, and local deformations were below the permissible standards.

The stresses on the radial direction were investigated to ascertain it effects on variations in the selected materials properties. It was discovered that these factors have a substantial effect on the stresses in both the tube and shell made of AL-6XN that were subjected to high heat flow, internal pressure and fluctuating temperatures, particularly in the axial directions. Regarding the ability of numerous baffles to increase temperature values as well as the low stress and minimal deformational properties of AL-6XN in the new design, WKX110 appears to be a more acceptable solution to the primary corrosion problems PMX110 encountered. By

31

analyzing actual operational data from installed equipment, the applicability of the suggested model was assessed. The outcomes demonstrated that the propound heat exchanger's stress, strain and deformations met ASME specifications. The primary contribution of this study is the recommendation of a novel material that will aid in the elimination of high-temperature corrosion induced by the abundance of potassium and chloride in biomass. A comprehensive experimental study between the current materials under consideration to better understand both physical and mechanical behaviour of these metals.

DISCLAIMER (ARTIFICIAL INTELLIGENCE)

Author(s) hereby declare that NO generative AI technologies such as Large Language Models (ChatGPT, COPILOT, etc) and text-to-image generators have been used during writing or editing of manuscripts.

COMPETING INTERESTS

Authors have declared that no competing interests exist.

REFERENCES

1. Pandiyarajan V, Pandian MC, Malan E, Velraj R, Seeniraj R. Experimental investigation on heat recovery from diesel engine exhaust using finned shell and tube heat exchanger and thermal storage system. Applied Energy. 2011;88(1):77-87.
2. Saidur R, Rezaei M, Muzammil WK, Hassan M, Paria S, Hasanuzzaman M. Technologies to recover exhaust heat from internal combustion engines. Renewable and Sustainable Energy Reviews. 2012;16 (8):5649-5659.
3. Dolz V, Novella R, García A, Sánchez J. HD Diesel engine equipped with a bottoming Rankine cycle as a waste heat recovery system. Part 1: Study and analysis of the waste heat energy. Applied Thermal Engineering. 2012;36:269-278.
4. Zhu S, Deng K, Qu S. Energy and exergy analyses of a bottoming Rankine cycle for engine exhaust heat recovery. Energy. 2013;58:448-457.
5. Samal AK. Shell and tube heat exchanger design using CFD Tools; 2013.
6. Salahuddin U, Bilal M, Ejaz H. A review of the advancements made in helical baffles used in shell and tube heat exchangers. International Communications in Heat and Mass Transfer. 2015;67:104-108.
7. Guerras LS, Martín M. On the water footprint in power production: Sustainable design of wet cooling towers. Applied Energy. 2020;263:114620.
8. Westerlund L, Hermansson R, Fagerström J. Flue gas purification and heat recovery: A biomass fired boiler supplied with an open absorption system. Applied Energy. 2012;96:444-450
9. Asteman H, Svensson JE, Norell M, Johansson LG. Influence of water vapor and flow rate on the high-temperature oxidation of 304L; effect of chromium oxide hydroxide evaporation. Oxidation of Metals. 2000;54:11-26.
10. Halvarsson M, Tang JE, Asteman H, Svensson JE, Johansson LG. Microstructural investigation of the breakdown of the protective oxide scale on a 304 steel in the presence of oxygen and water vapour at 600 C. Corrosion Science. 2006;48(8):2014-2035.
11. Folkeson N, Pettersson J, Pettersson C, Johansson LG, Skog E, Andersson BÅ, Enestam S, Tuiremo J, Jonasson A, Heikne B. Fireside corrosion of stainless and low alloyed steels in a waste-fired CFB boiler; The effect of adding sulphur to the fuel. Materials Science Forum; 2008.
12. Nielsen HP, Frandsen F, Dam-Johansen K, Baxter L. The implications of chlorine-associated corrosion on the operation of biomass-fired boilers. Progress in Energy and Combustion Science. 2000;26(3):283-298.
13. Broström M, Kassman H, Helgesson A, Berg M, Andersson C, Backman R, Nordin A. Sulfation of corrosive alkali chlorides by ammonium sulfate in a biomass fired CFB boiler. Fuel Processing Technology. 2007; 88(11-12):1171-1177.
14. Viklund P, Pettersson R, Hjörnhede A, Henderson P, Sjövall P. Effect of sulphur containing additive on initial corrosion of superheater tubes in waste fired boiler. Corrosion Engineering, Science and Technology. 2009;44(3):234-240.
15. Pettersson A, Åmand LE, Steenari BM. Chemical fractionation for the characterisation of fly ashes from co-combustion of biofuels using different methods for alkali reduction. Fuel. 2009;88 (9):1758-1772.
16. Simms N, Kilgallon P, Oakey J. Degradation of heat exchanger materials

under biomass co-firing conditions. Materials at High Temperatures. 2007;24 (4):333-342.

17. Alamu SO, Lee SW, Qian X. Exergy and Energy Analysis of the Shell-and-Tube Heat Exchanger for a Poultry Litter Co-Combustion Process. *Processes.* 2023;*11*(8):2249.

18. Mori S, Sanusi T, Simms N, Sumner J. Fireside corrosion and deposition on heat exchangers in biomass combustion systems. Materials at High Temperatures. 2023;40(1):36-47.

19. Nsofor EC, Celik S, Wang X. Experimental study on the heat transfer at the heat exchanger of the thermoacoustic refrigerating system. Applied Thermal Engineering. 2007;27(14-15):2435-2442.

20. Alperen MA, Kayabaşi E, Kurt H. Detailed comparison of the methods used in the heat transfer coefficient and pressure loss calculation of shell side of shell and tube heat exchangers with the experimental results. Energy Sources, Part A: Recovery, Utilization, and Environmental Effects. 2019;1-20.

21. Ozden E, Tari I. Shell side CFD analysis of a small shell-and-tube heat exchanger. Energy Conversion and Management. 2010;51(5):1004-1014.

22. Pal E, Kumar I, Joshi JB, Maheshwari N. CFD simulations of shell-side flow in a shell-and-tube type heat exchanger with and without baffles. Chemical Engineering Science. 2016;143, 314-340.

23. Jorge L, Righetto A, Polli P, Santos O, Maciel Filho R. Simulation and analysis of a sugarcane juice evaporation system. Journal of Food Engineering. 2010; 99(3):351-359.

24. Ranjbar-Far M, Absi J, Mariaux G, Dubois F. Simulation of the effect of material properties and interface roughness on the stress distribution in thermal barrier coatings using finite element method. Materials & Design. 2010;31(2):772-781.

25. Białas M. Finite element analysis of stress distribution in thermal barrier coatings. Surface and Coatings Technology. 2008; 202(24):6002-6010.
Available:https://doi.org/https://doi.org/10.1016/j.surfcoat.2008.06.178

26. Evans AG, Mumm DR, Hutchinson JW, Meier GH, Pettit FS. Mechanisms controlling the durability of thermal barrier coatings. Progress in Materials Science. 2001;46(5):505-553.
Available:https://doi.org/https://doi.org/10.1016/S0079-6425(00)00020-7

27. Pettersson J, Svensson JE, Johansson LG. KCl-induced corrosion of a 304-type austenitic stainless steel in O_2 and in O_2+ H_2O environment: the influence of temperature. Oxidation of Metals. 2009;72: 159-177.

Peer-review history:
The peer review history for this paper can be accessed here:
https://www.sdiarticle5.com/review-history/119904